

Current-fluctuation spectra of liquid rubidium

J. Bosse, W. Götze, and M. Lücke

Max-Planck-Institut für Physik und Astrophysik, D-8000 München, Germany
and Physik-Department der Technischen Universität München, 8046 Garching, Germany

(Received 3 March 1978)

The mode-coupling theory has been worked out to calculate the longitudinal and transverse current-fluctuation spectra, the dynamical structure factor, and the dynamical as well as the static transport coefficients of liquid rubidium. The results are compared with experimental data. A detailed comparison of the excitation spectra of liquid rubidium with those of liquid argon is presented.

I. INTRODUCTION

The density-fluctuation spectrum of liquid rubidium has recently been studied by inelastic neutron scattering^{1,2} and by molecular-dynamics (MD) simulations.^{3,4} The most interesting feature predicted by the MD calculations and observed in the neutron scattering experiments is the persistence of propagating density fluctuations up to wave numbers of 1.2 \AA^{-1} . The wavelength of these density oscillations in rubidium is only slightly larger than the average interparticle distance, whereas experiments for liquid argon displayed propagating density fluctuations only with wavelengths larger than six times the interparticle spacing.³ There have been a number of theoretical attempts to reproduce the behavior of the Van Hove function of liquid Rb (Refs. 5 and 6) and to explain the appearance of short-wavelength density excitations^{5,7} in the past.⁸ In this paper, we report the results of an application of the mode-coupling theory of simple classical liquids⁹ to liquid rubidium. This theory, which has already been used to analyze the dynamics of liquid argon, will be demonstrated to represent an adequate framework to explain also the liquid-rubidium dynamics as well as to obtain satisfactory numerical results for the correlation functions.

The input data for our numerical calculations, number density $n = 1.06 \times 10^{22} \text{ cm}^{-3}$, particle mass $m = 141.9 \times 10^{-24} \text{ g}$, and temperature $T = 319 \text{ °K}$, define the thermodynamic state which Rahman⁴ simulated in his MD experiment. We also use the effective pair potential for the ionic motion derived by Price *et al.*¹⁰ with the well depth $\epsilon = 402.7 k_B \text{ °K}$ and the hard-core extension $\sigma = 4.4 \text{ \AA}$. The theory requires as further input the pair distribution function $g(r)$ which is for convenience taken from Rahman's work together with the structure factor $S(q)$.¹¹

The normalized correlation function of transverse current fluctuations is written

$$\phi_T(q, z) = \frac{-1}{z + q^2 D_T(q, z)}, \quad (1)$$

and

$$\phi_L(q, z) = \frac{-z}{z^2 - \Omega_0^2(q) + zq^2 D_L(q, z)} \quad (2)$$

denotes the longitudinal counterpart. The characteristic frequency $\Omega_0(q) = v_{\text{th}} q / [S(q)]^{1/2}$ measures the restoring force against static compressions of wave number q . Its long wavelength behavior is determined by the isothermal sound velocity $c_{\text{isoth}} = v_{\text{th}} / [S(q \rightarrow 0)]^{1/2}$ with $v_{\text{th}}^2 = k_B T / m$. The generalized transport coefficients $D_{L,T}(q, z)$ are represented in terms of relaxation kernels $M_{L,T}(q, z)$,

$$q^2 D_T(q, z) = -\Omega_T^2(q) / [z + M_T(q, z)], \quad (3)$$

$$q^2 D_L(q, z) = -\Delta^2(q) / [z + M_L(q, z)], \quad (4)$$

with $\Delta^2(q) = \Omega_L^2(q) - \Omega_0^2(q)$. The second frequency moments $\Omega_{L,T}^2(q)$ (Ref. 12) of the current excitation spectra are determined by the second derivatives of the potential and $g(r)$.

The absorptive parts $M_{L,T}''(q, \omega)$ of the relaxation kernels are given by the Fourier transform of the correlation function of the fluctuating forces. This spectrum $M_{L,T}''(q, \omega)$ is approximated within the mode-coupling theory⁹ by the decay spectrum of the mode into two others. There are two different decay channels: one into a longitudinal and a transverse mode and another into two longitudinal modes. These contributions to $M_{L,T}''(q, \omega)$ have a typical golden-rule form with the decay probability given by a vertex and by the density of final states allowed by energy and momentum conservation. Longitudinal and transverse modes are coupled via these decay processes. For details see Ref. 9.

In the zero wave number limit, $D_{L,T}(q, z)$ reduces to the dynamical transport coefficients $D_{L,T}(z)$ whose absorptive parts $D_{L,T}''(\omega)$ are the fluctuation spectra of the stress tensor. Van Hove's neutron scattering function is related to $\phi_L''(q, \omega)$ by

$$S(q, \omega) = \pi^{-1} \frac{v_{\text{th}}^2 q^2}{\omega^2} \phi_L''(q, \omega). \quad (5)$$

II. RESULTS

The peak structure of the relaxation kernels $M_{L,T}''(q, \omega)$ shown for three representative wave numbers in Fig. 1 is a consequence of the mode decay kinematics: the contribution to $M_{L,T}''(q, \omega)$ from the decay channel into one longitudinal and one transverse mode is a slowly decreasing function of frequency. But the contribution from two longitudinal modes increases with ω since the phase space for these decay products increases, and it exhibits a maximum around the Einstein frequency Ω_E . The relative importance of the two decay channels contributing to $M_{L,T}''(q, \omega)$ also depends on wave number q . While, for $q \gtrsim q_0 = 1.5 \text{ \AA}^{-1}$, both contributions have comparable frequency-maximum values, the longitudinal-transverse channel becomes less important for $q < q_0$. However, for very small q and ω the latter contribution determines the values of the transport coefficients according to Eqs. (74)–(76) of Ref. 9, while the longitudinal contribution vanishes in this limit.

The longitudinal relaxation spectrum $M_L''(q, \omega)$ is larger than $M_T''(q, \omega)$, a fact which is related to the different size of the longitudinal and transverse decay vertices [c.f. Eqs. (48c) and (53) of Ref. 9]. The longitudinal (transverse) functions are dominated by the longitudinal (transverse) part of the tensor of second derivatives of the potential.

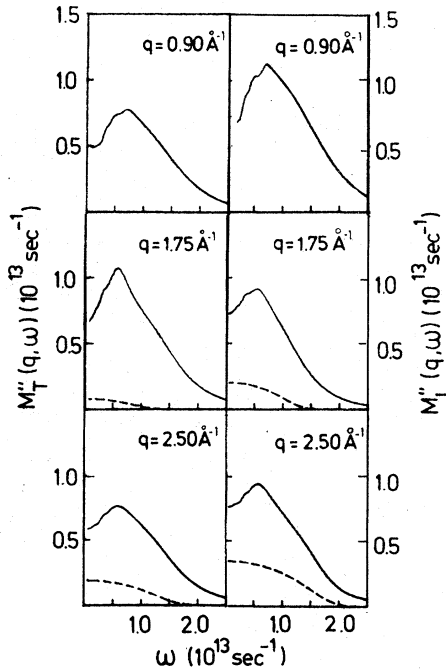


FIG. 1. Relaxation spectra $M''(q, \omega)$ for the transverse and longitudinal current fluctuations. The dashed curves represent the free-gas contribution.

The longitudinal part of this tensor being, on the average, larger than its transverse part explains the difference.

The generalized transport coefficients $D_{L,T}''(q, \omega)$ [Eqs. (3) and (4)] exhibit a two-peak structure. There is a rather broad side peak roughly defined by the average value of $M''(q, \omega)$ and a narrow low-frequency peak due to the dip of $M''(q, \omega)$ for $\omega \rightarrow 0$. This frequency behavior of $D_{L,T}''(q, \omega)$ again reflects the basic mode-coupling dynamics which suppresses the decay of low-frequency modes into two longitudinal excitations and enhances the decay at intermediate frequencies (c.f. Fig. 1). The above-described features of $D_{L,T}''(q, \omega)$ are most clearly seen for the case $q=0$ shown in Fig. 2. The static transport coefficients are obtained as

$$\eta = nmD_T''(0, 0) = 7.8 \times 10^{-3} \text{ P},$$

$$\Gamma_L = nmD_L''(0, 0) = 17.6 \times 10^{-3} \text{ P}.$$

These numbers were calculated from Eqs. (74)–(76) of Ref. 9 using $c_T = [\Omega_T(q)/q]_{q=0} = 857 \text{ m sec}^{-1}$, $c_L = [\Omega_L(q)/q]_{q=0} = 1602 \text{ m sec}^{-1}$, and $c_{\text{isoth}} = [\Omega_0(q)/$

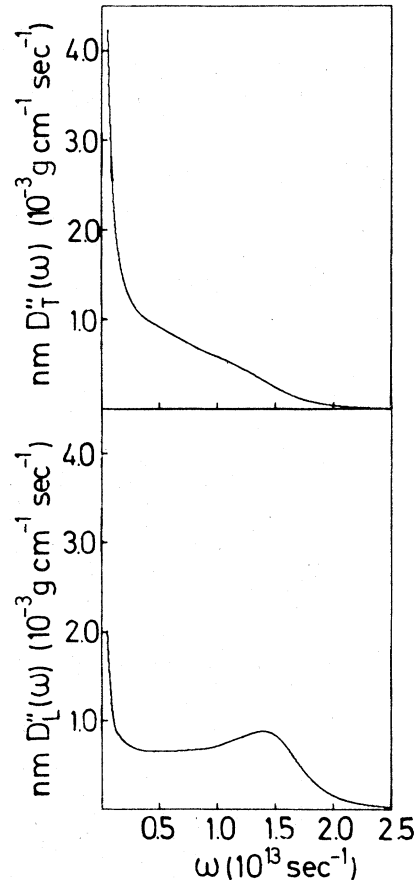


FIG. 2. Dynamical-transport coefficients as functions of frequency.

$q]_{q=0} = 1137 \text{ m sec}^{-1}$. The velocities $c_{T,L}$ were determined according to Eqs. (16) and (41) of Ref. 9 using Rahman's pair-distribution function $g(r)$. Unfortunately, there are no molecular-dynamics results available at present for the viscosities to compare with.

Substitution of Eq. (3) into Eq. (1) yields the typical response function for an oscillator with a restoring force measured by $\Omega_T(q)$ and with a damping function $M_T(q, z)$,

$$\phi_T(q, z) = -\frac{z + M_T(q, z)}{z^2 - \Omega_T^2(q) + zM_T(q, z)}, \quad (6)$$

$$\phi_T''(q, \omega) = \Omega_T^2(q) \frac{M_T''(q, \omega)}{[\omega^2 - \Omega_T^2(q) + \omega M_T'(q, \omega)]^2 + [\omega M_T''(q, \omega)]^2}. \quad (7)$$

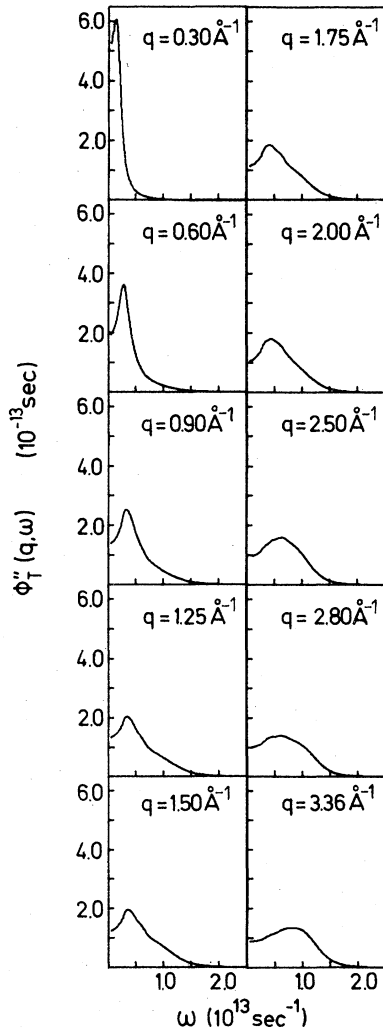


FIG. 3. Spectrum of transverse current fluctuations.

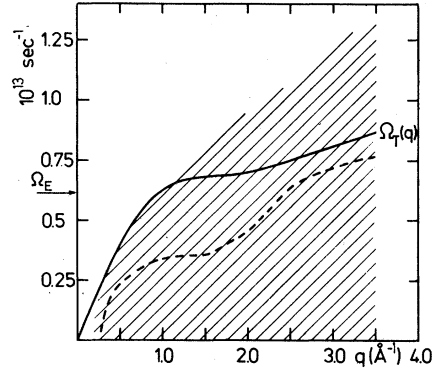


FIG. 4. Frequency of shear modes (dashed curve) compared to $\Omega_T(q)$ (full curve). Within the shaded area, the transverse current excitation spectrum drops to half maximum value.

Note that $M_T''(q, \omega)$ is for most frequencies of the order of $\Omega_T(q)$ and thus resonances are not defined by zeros in the real part of the denominator of Eq. (6) but rather by the minimum of the denominator of Eq. (7). The resonance height is determined by the inverse minimal size of the denominator. The increase of the latter as a function of q explains the decrease in peak height of the spectrum of transverse current fluctuations shown in Fig. 3. The monotonically increasing resonance width is due to the peak structure of $M_T''(q, \omega)$ becoming broader: this behavior implies directly and via the real part $M_T'(q, \omega)$ that the minimum of the denominator in Eq. (7) becomes broader. This effect causes the resonance of $\phi_T''(q, \omega)$ to vanish for large q . For small wave numbers, where the damping M_T'' is much larger than the restoring force Ω_T , the current fluctuations exhibit hydrodynamic behavior, i.e., $\phi_T''(q, \omega)$ has a narrow central diffusion

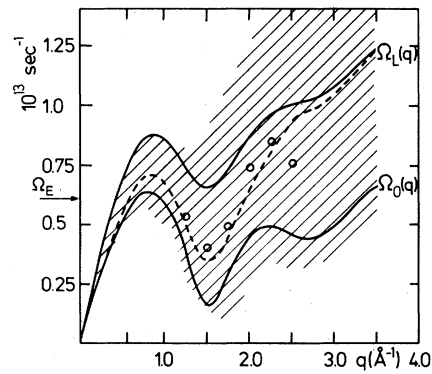


FIG. 5. Peak positions of the longitudinal-current-fluctuation spectra (dashed curve) in comparison with $\Omega_L(q)$ and $\Omega_0(q)$. Within the shaded area the current spectra drop to half maximum values. Circles denote neutron scattering results (Ref. 2).

peak produced by a well-defined minimum of the denominator of Eq. (7) at zero frequency.

The dispersion law of the strongly damped shear modes is plotted in Fig. 4 as a function of wave number in comparison with $\Omega_T(q)$. Since the real part of the relaxation kernel $M_T^*(q, \omega)$ displays normal dispersion in the frequency range of interest, the resonance of $\phi_T^*(q, \omega)$ is pushed below $\Omega_T(q)$. This is a level repulsion effect between the bare transverse mode of frequency $\Omega_T(q)$ and the spectrum of coupled density and transverse shear excitations in $M_T^*(q, \omega)$ which is peaked around Ω_E . The strong level repulsion—in the wave number range between 0.5 and 2 \AA^{-1} the actual oscillation frequency is only half as big as Ω_T —can also be interpreted with pictures used in the theory of quantum liquids¹³: The absorptive part $M_T^*(q, \omega)$ is due to excitations of pairs of modes and the real part $M_T'(q, \omega)$ describes the effect of the backflow produced by pair excitations on the mode. The backflow yields an increase of inertia and hence a decrease of the resonance frequency. In this picture, the transition of the propagating shear mode to an overdamped or diffusive one is caused by the backflow drag becoming too strong compared with the restoring force Ω_T .

The structure of the longitudinal current-fluctuation spectrum is quite different from the transverse one. Mathematically, this is caused by $q^2 D_L(q, z)$ entering Eq. (2) at a place where in the transverse case [Eq. (6)] the kernel $M_T(q, z)$ enters

$$\phi_L^*(q, \omega) = \omega^2 \frac{q^2 D_L^*(q, \omega)}{[\omega^2 - \Omega_0^2(q) + \omega q^2 D_L^*(q, \omega)]^2 + [\omega q^2 D_L^*(q, \omega)]^2} \quad (8)$$

The well-known physical reason for this more-complicated structure of the longitudinal current-correlation function is discussed in Ref. 9. Since $D_L^*(q, \omega)$, in contrast to $M_T^*(q, \omega)$, is peaked at zero frequency, $D_L^*(q, \omega)$ is for small frequencies negative, decreasing with ω . For large frequencies it approaches zero. Hence, the first bracket in the denominator of Eq. (8) has a zero above $\Omega_0(q)$ reflecting the repulsion of the bare resonance $\Omega_0(q)$ to a higher frequency due to the low-frequency resonance of $D_L^*(q, \omega)$. Thus, the peak position of the spectrum $\phi_L^*(q, \omega)$ as shown in Fig. 5 is somewhat above $\Omega_0(q)$ for small q . The repulsion effect is still enhanced due to the factor ω^2 in the numerator of Eq. (8). As q is increased this ω^2 factor is responsible for $\phi_L^*(q, \omega)$ continuing to show a peak structure, even though the denominator increases monotonically as a function of ω . For large q , the peak position in $\phi_L^*(q, \omega)$ is expected

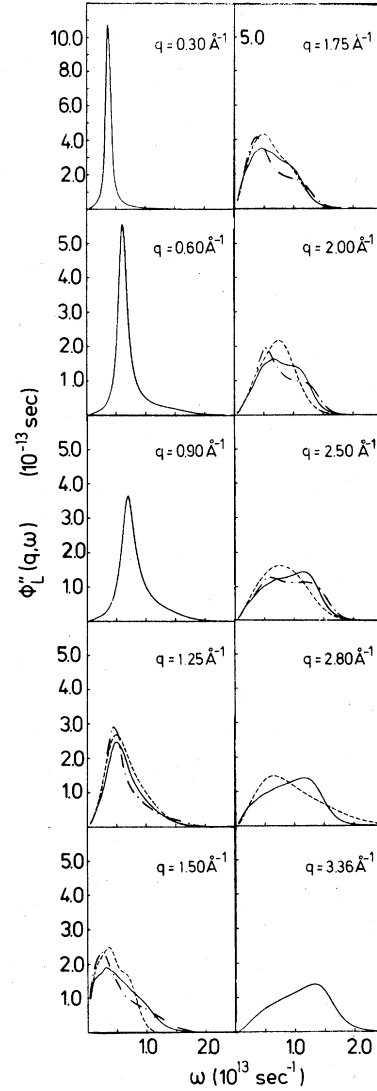


FIG. 6. Longitudinal-current-fluctuation spectra of the present theory (full curves) compared with neutron-scattering results of Copley and Rowe (Ref. 2) (dashed curves). Dash-dotted curves represent our theoretical result with Rahman's $S(q)$ (Ref. 4) replaced by $S(q)$ obtained from neutron scattering (Ref. 5).

at $\sqrt{2}v_{th}q$, while $\Omega_L(q) \rightarrow \sqrt{3}v_{th}q$ and $\Omega_0(q) \rightarrow v_{th}q$ (ideal gas behavior). The resonance positions are in satisfactory agreement with the neutron scattering data.²

Figure 6 shows the longitudinal-current-fluctuation spectra in comparison with neutron scattering results.² For wave numbers between 1.25 and 2.5 \AA^{-1} there is satisfactory agreement with experiment. Since Rahman's structure factor differs from the one obtained by neutron scattering, we show also (dash-dotted lines in Fig. 6) the results of our theory for $\phi_L^*(q, \omega)$ with Rahman's $S(q)$ replaced by the experimental $S(q)$.⁵ In Fig. 7, the

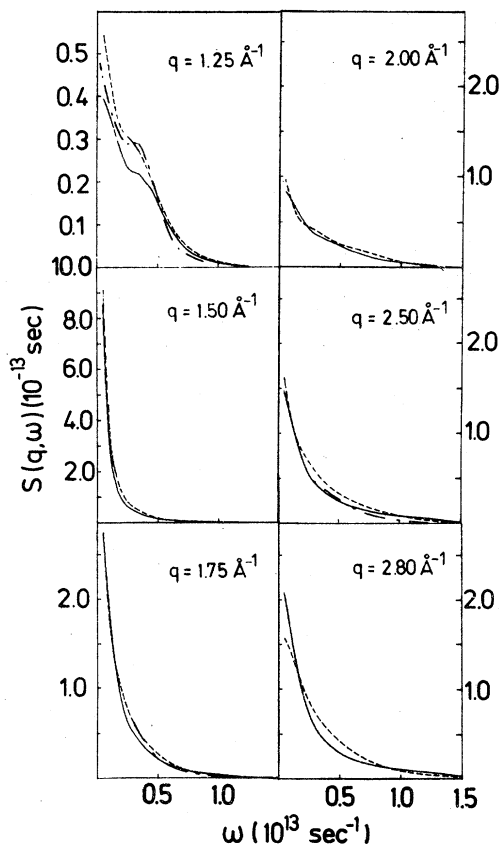


FIG. 7. Dynamical structure factor $S(q, \omega)$ of liquid rubidium. The meaning of the different curves is the same as in Fig. 6.

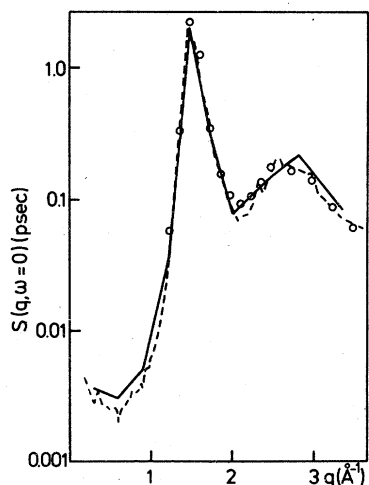


FIG. 8. Zero-frequency limit of the dynamical structure factor ($\omega=0$) in comparison with MD results (dashed curve) and neutron scattering data (circles).

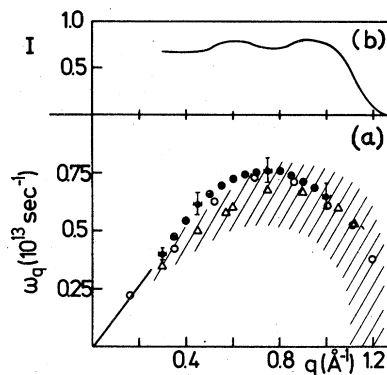


FIG. 9. (a) Density fluctuation frequency ω_q . Full circles represent MD results (Ref. 3), open circles denote neutron scattering data (Ref. 1), and triangles represent the theory. Within the shaded area the theoretical $S(q, \omega)$ drops to its half maximum value. (b) Relative area of $S(q, \omega)$ under the peak at ω_q .

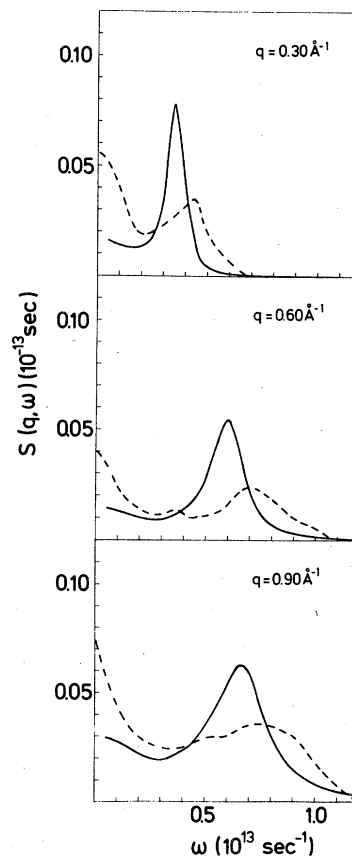


FIG. 10. Dynamical structure factor for small wave numbers in comparison with neutron scattering results (Ref. 1) (dashed curves).

theoretical density-fluctuation spectrum is compared with the experimental one for intermediate wave numbers. The zero-frequency intensity of density fluctuations is shown in Fig. 8. The agreement between theory and experiment in Figs. 7 and 8 is satisfactory, but these plots are not a very sensitive test for a theory.

Since the longitudinal-current-fluctuation spectra exhibit very sharp resonances for $q < 1 \text{ \AA}^{-1}$, Van Hove's correlation function $S(q, \omega)$ shows well-defined resonance peaks representing propagating density fluctuations. The dispersion law for these modes and their relative contribution to the total spectrum $S(q, \omega)$ of density excitations are shown in Fig. 9.

As shown in Fig. 10 in more detail, the present theory yields excitation energies for the collective density modes being somewhat below the experimental data¹ with resonance widths sharper than the experimental ones. We suspect the neglect of coupling to energy fluctuations to be responsible for this.

III. ARGON VERSUS RUBIDIUM

The mode-coupling theory brings out some typical differences between the excitation spectra of liquid rubidium and liquid argon even though there is some correspondence between their states. After scaling energies with the Einstein frequency ($\Omega_E^{\text{Ar}} \approx 0.74 \times 10^{13} \text{ sec}^{-1}$; $\Omega_E^{\text{Rb}} \approx 0.61 \times 10^{13} \text{ sec}^{-1}$, and wave vectors with the peak position q_0 of $S(q)$ ($q_0^{\text{Ar}} \approx 2 \text{ \AA}^{-1}$; $q_0^{\text{Rb}} \approx 1.5 \text{ \AA}^{-1}$) the structure factor and the characteristic frequencies $\Omega_{L,T}(q)$ are quite similar in both liquids. The most conspicuous difference in static behavior and also the most influential one upon the dynamics is the different compressibility manifesting itself in smaller long wavelength values of $S(q)$ in rubidium. The much larger stiffness of rubidium for $q < \frac{1}{2}q_0$ implies $\Omega_0(q)$ to be considerably larger in rubidium than in argon and, by the same token, $\Delta^2(q) = \Omega_L^2(q) - \Omega_0^2(q)$ to be smaller by a factor of 2 to 3 compared to argon in the wave number range up to $\frac{1}{2}q_0$. For $q \approx q_0$, however, static restoring forces $\Omega_0(q)$ are similar in both liquids. Consequently, rubidium shows a steeper ascent of $\Omega_0(q)$ for $q \lesssim \frac{1}{2}q_0$ and a more oscillatory behavior between $q = 0$ and q_0 .

The resonance $\omega_L(q)$ of longitudinal current fluctuations is located between $\Omega_L(q)$ and $\Omega_0(q)$, and, thus, $\omega_L(q)/\Omega_E$ of rubidium is not only larger and steeper for $q \lesssim \frac{1}{2}q_0$, but exhibits also a more-pronounced oscillation than in argon. These features imply a smaller density of longitudinal states in rubidium. Since the density of final states for decay modes crucially enters in our theory for the fluctuating-force spectrum $N''(q, \omega)$ [see Ref. 9,

Eqs. (45)–(51)], one expects this basic quantity of the theory to be smaller in rubidium than in argon. Our numerical results for $N''_{L,T}(q, \omega)$ in argon are indeed almost twice as big as in rubidium for $q \lesssim \frac{1}{2}q_0$. The enhancement of the relaxation mechanism $N''_T(q, \omega)$ in argon explains why the transverse low-frequency transport coefficient

$$D_T''(\omega) = c_T^4 / [N_T''(q, \omega) / q^2]_{q=0},$$

and hence the shear viscosity of argon is smaller than that of rubidium.

For the longitudinal low-frequency transport coefficient

$$D_L''(\omega) = (c_L^2 - c_{\text{isoth}}^2) / [N_L''(q, \omega) / q^2]_{q=0},$$

both numerator and denominator are larger in argon than in rubidium. However, the much stronger effect of

$$(c_L^2 - c_{\text{isoth}}^2) = [\Delta^2(q) / q^2]_{q=0}$$

overcompensates the difference between the spectra $N_L''(q, \omega)$ of rubidium and argon. And so the longitudinal low-frequency transport coefficient, i.e., the sound damping is larger in argon.

$N''(q, \omega)$ shows a peak essentially due to the peak in the longitudinal density of states. The energy $\omega_L(\frac{1}{2}q_0)$ of the longitudinal modes with zero group velocity being larger in rubidium than in argon ($1.2 \Omega_E$ vs $0.8 \Omega_E$) implies (i) that the former peak is shifted to higher energies in rubidium and (ii) that $N''(q, \omega)$ extends to higher frequencies in rubidium than in argon.

The transverse relaxation spectra at their maxima $M_T''/\Omega_E = N_T''/(\Omega_T^2\Omega_E)$ are more or less of equal height in both liquids because the difference in magnitude of $N_T''(q, \omega)$ is roughly compensated by the different size of Ω_E . Their shape however differs decisively: not only is the peak position of $M_T''(q, \omega)$ in rubidium shifted to slightly a higher frequency but, more important, its half width is well above the width $2\Omega_E$ of the argon spectrum as mentioned before. So the two-mode spectrum $M_T''(q, \omega)$ of argon shows better-defined excitation peaks than that of rubidium. Together with the deeper minimum of $M_T''(q, \omega)$ implied by the steeper decrease of the peak in $M_T''(q, \omega)$, this leads in the spectrum $D_T''(q, \omega)$ of argon to a stronger hybridization on the high-frequency side ($\omega > \Omega_E$) with the two mode levels peaked at $\omega \approx \Omega_E$. Thus, the high-frequency shoulder in $D_T''(q, \omega)$ is more pronounced in argon than in rubidium. The larger high-frequency damping $D_T''(q, \omega)$ in argon finally leads to resonances in $\phi_T''(q, \omega)$ which are on the high-frequency side broader in argon than in rubidium.

With regard to the high-frequency shoulder in the longitudinal dynamical-transport coefficient $D_L''(q, \omega)$, one finds the opposite situation to the

transverse case discussed above: $D_L''(q, \omega)$ exhibits a better-defined high-frequency shoulder (or peak) in rubidium. The ultimate reason for this is the much-smaller rubidium value of Δ^2 which dominates in

$$M_L''(q, \omega)/\Omega_E = N_L''(q, \omega)/(\Delta^2 \Omega_E)$$

so much that it overcompensates considerably the smaller rubidium $N_L''(q, \omega)$. The much-larger two-mode spectrum $M_L''(q, \omega)$ in rubidium—although being broader than in argon—entails a lower minimum of $M_L''(q, \omega)$ at the high-frequency falloff in $M_L''(q, \omega)$. Both effects lead, as explained above, to a stronger high-frequency hybridization with the two mode levels of $M_L''(q, \omega)$, i.e., the high-frequency shoulder in $D_L''(q, \omega)$ around $2\Omega_E$ is more pronounced in rubidium. It would be interesting to check the predictions of the present theory concerning the different high-frequency-shoulder structures in the generalized dynamical-transports coefficients $D_{L,T}''(q, \omega)$ against MD experiments.

As explained above, $M_L''(q, \omega)/\Omega_E$ is considerably larger in rubidium than in argon. This together with $\Delta^2(q)$ being smaller in rubidium implies that $D_L''(q, \omega)$ is smaller in rubidium. And so, according to Eq. (2), the longitudinal resonance of rubidium is close to $\Omega_0(q)$ for $q \lesssim q_0$, i.e., the situation corresponds to the fast-relaxation or motional-

narrowing regime [$M_L''(q, \omega)$ large]. With increasing q , the resonance width increases, and there is a monotonic transition to the slow-relaxation regime: for q exceeding q_0 , $M_L''(q, \omega)$ becomes small enough in rubidium that the longitudinal resonance in Fig. 5 shifts close to $\Omega_L(q)$.

Argon, on the other hand, displays the slow relaxation [$\omega_L(q)$ approaching $\Omega_L(q)$] not only for large $q > q_0$ but also for wave numbers around $\frac{1}{2}q_0$. For $q \lesssim \frac{1}{4}q_0$ and for $q \sim q_0$, however, the longitudinal resonance frequency $\omega_L(q)$ of argon is closer to $\Omega_0(q)$. Thus, the mode damping is nonmonotonic as a function of q . A further consequence of these differences is that the relative lifetime of longitudinal modes, i.e., the resonance frequency divided by the resonance width, is larger in rubidium than in argon. As a result, the rubidium resonances show up in $S(q, \omega)$ for q as large as 1.2 \AA^{-1} .

In summary, one can say that the smaller compressibility of rubidium causes the dynamical behavior of liquid rubidium to be more solidlike than that of liquid argon.

ACKNOWLEDGMENT

The authors are grateful to A. Rahman, who supplied them with a list of tables for the pair potential, the pair distribution function, and the structure factor.

¹J. R. D. Copley and J. M. Rowe, Phys. Rev. Lett. **32**, 49 (1974).

²J. R. D. Copley and J. M. Rowe, Phys. Rev. A **9**, 1656 (1974); a table of results for $S(q, \omega)$ is published in Ref. 5.

³A. Rahman, Phys. Rev. Lett. **32**, 52 (1974).

⁴A. Rahman, Phys. Rev. A **9**, 1667 (1974).

⁵J. R. D. Copley and S. W. Lovesey, Rep. Prog. Phys. **38**, 461 (1975).

⁶R. Bansal and K. N. Pathak, Phys. Rev. A **11**, 1450 (1975); M. I. Barker and T. Gaskell, J. Phys. (Paris) C **8**, 89 (1975); **8**, 3715 (1975); P. K. Kahol, R. Bansal, and K. N. Pathak, Phys. Rev. A **14**, 408 (1976); O. Chiakwelu, T. Gaskell, and J. W. Tucker, J. Phys. (Paris) C **9**, 1635 (1976).

⁷J. N. E. Lewis and S. W. Lovesey, J. Phys. (Paris) C **10**, 3221 (1977).

⁸Very recently L. Sjögren and A. Sjölander [Ann. Phys.

(N.Y.) **110**, 421 (1978)] published results on density fluctuations in liquid rubidium which are in qualitative agreement with experiment. As their theory starts from a kinetic-equation approach it is difficult to compare their approximations to the mode-coupling approximation used in the present work.

⁹J. Bosse, W. Götze, and M. Lücke, Phys. Rev. A **17**, 434 (1978); **17**, 447 (1978).

¹⁰D. L. Price, K. S. Singwi, and M. P. Tosi, Phys. Rev. B **2**, 2983 (1970); D. L. Price, Phys. Rev. A **4**, 358 (1971).

¹¹A. Rahman (private communication).

¹²The reader is referred to Ref. 5 for a review of the theoretical concepts as well as the experimental situation of simple classical liquids.

¹³R. P. Feynman, *Statistical Mechanics, A Set of Lectures* (Benjamin, Reading, Mass., 1972); W. Götze and M. Lücke, Phys. Rev. B **13**, 3825 (1976).